Available online at www.sciencedirect.com
SCIENCE DIRECT®
Journal of Marine Systems 49 (2004) 3–18
JOURNAL OF MARINE SYSTEMS
www.elsevier.com/locate/jmarsys

A proposed mechanism for turbulent enhancement of broadcast spawning efficiency

J.P. Crimaldi*, H.S. Browning

Department of Civil, Environmental, and Architectural Engineering, University of Colorado, Boulder, CO 80309-0428, USA

Received 16 October 2002; accepted 6 June 2003
Available online 14 August 2004

Abstract

The broadcast spawning reproductive strategy relies on turbulent-stirring processes in the flow to bring together gametes previously released by adult males and females. The subsequent fertilization rate depends on the product of co-occurring concentrations of egg and sperm. Turbulent mixing produces a strong average dilution in these concentrations, suggesting that an increase in turbulence would reduce the average local fertilization rate. However, turbulent dilution occurs at time scales that may be long compared to those associated with fertilization. Therefore, the instantaneous structure of egg and sperm filaments at shorter time scales must be considered. In this paper, a mechanism is proposed whereby coherent turbulent structures in the velocity field cause coalescence between high-concentration filaments of egg and sperm, significantly enhancing the average fertilization rate. Simple analytical and numerical models are used to demonstrate how the mechanism works, and to make qualitative estimates of its effect on the resulting fertilization rate. The results suggest that the efficiency of broadcast spawning is a consequence of features in the instantaneous turbulent field, and that this efficiency is not captured by models that consider only time-averaged features of the flow.

Keywords: Turbulence; Turbulent diffusion; Plumes; Benthic boundary layer; Spawning; External fertilization

1. Introduction

Many benthic invertebrates utilize broadcast spawning as a reproductive strategy. Species using this type of external fertilization are typically sessile (e.g., mussels, sea urchins, sea anemones, tube-dwelling polychaetes), or are limited in their ability to aggregate by the nature of their chosen habitats or environments (Denny and Shibata, 1989). To spawn, adult males and females extrude sperm and ova into the surrounding flow, typically a turbulent benthic boundary layer. The strategy then relies primarily on turbulent stirring (at large and moderate spatial scales) and molecular diffusion and sperm taxis (at small scales) to bring the gametes together before possible fertilization can take place. Locally, the fertilization rate depends on the product of co-occurring egg and sperm concentrations (Vogel et al., 1982), and these concentration fields are largely shaped by the characteristics of the turbulent stirring. Conventional thought has been that, because turbulence rapidly dilutes the

* Corresponding author. Tel.: +1-303-7352162; fax: +1-303-4927317.
E-mail address: crimaldi@colorado.edu (J.P. Crimaldi).
URL: http://ceae.Colorado.EDU/~crimaldi/.

0924-7963/$ - see front matter © 2004 Elsevier B.V. All rights reserved.
doi:10.1016/j.jmarsys.2003.06.005

concentrations of egg and sperm, it diminishes the effectiveness of broadcast spawning. Current models (Denny, 1988; Denny and Shibata, 1989) support this concept, but these models strongly underpredict measured fertilization rates in the field. In this paper, we propose a contrary hypothesis as follows. While turbulence promotes dilution at longer time scales (and in an averaged sense), instantaneous turbulent processes might promote short-term coalescence of egg and sperm, enhancing fertilization rates. We use a combination of conceptual, analytical and numerical models to provide highly simplified illustrations of how these mechanisms might work. The purpose of this paper is not to provide definitive or quantitative answers to this problem; instead, we seek to suggest a new framework for studies concerning the role of turbulent stirring in the broadcast spawning process.

A range of physical, chemical, and biological factors affect the success of broadcast spawning. Most of these factors are beyond the scope of this paper; we focus here on the role of physical stirring of egg and sperm by fluid turbulence. Prior studies have identified a host of biological factors. The importance of adult aggregation and distribution has been shown in the field (Pennington, 1985; Coma and Lasker, 1997; Atkinson and Yund, 1996; Levitan et al., 1992), and with analytical models (Denny et al., 1992; Levitan and Young, 1995; Claereboudt, 1999). Adult synchronization of gamete release increases the likelihood of contact between egg and sperm, and mitigates deleterious effects of sperm aging (Giese and Pearse, 1974; Levitan et al., 1991; Levitan, 1995). The period of time over which the gametes are released, the individual reproductive output, and the collective ratio of sperm and ova also influence fertilization success (Yund, 2000). Once released into the flow, sperm and ova may coalesce as a result of passive transport by the turbulence, or by active sperm swimming. Sperm chemotaxis has been documented in several phyla (Miller, 1985), but the demonstrated attraction distance was only 100–200 mm. Sperm swimming velocities have been measured for several benthic invertebrates to be in the range of 0.05–0.3 mm s^{-1} (Gray, 1955; Levitan et al., 1991; Levitan, 1993). Because the separation between spawning adults may be on the scale of centimeters or meters, and the velocity fluctuations in typical turbulent benthic flows are on the scale of 0.01–0.1 m s^{-1} (Denny, 1988), it is likely that the motion of egg and sperm is almost entirely passive (Eckman, 1996). In addition, it has been suggested that the action of sperm swimming and chemotaxis is unlikely to substantially increase egg–sperm collisions (Levitan, 1995). However, if turbulent stirring brings the sperm and egg into close proximity, sperm swimming and chemotaxis might significantly increase the effective local mixing rates. Once a sperm–ova collision takes place, factors including sperm age, compatibility, and the jelly coat thickness of the egg determine if the collision will lead to a successful fertilization (Levitan, 1995). Even if fertilization does take place, other factors can impede the proper development of the zygote. The possible rapid refertilization of an egg by a second sperm leads to polyspermy and either mortality or abnormal larval development (Byrd and Collins, 1975; Styan, 1998). Excessive hydrodynamic shear has also been shown to impede normal development (Mead and Denny, 1995).

We now turn our attention to prior studies of the role of physical (turbulent) processes on fertilization success. Denny (1988) and Denny and Shibata (1989) developed an analytical model to investigate the effect of mean turbulent transport and dispersion on broadcast spawning. The model combines a fertilization kinetics model (Vogel et al., 1982) with a model for time-averaged plume concentrations (Csanady, 1973) to predict fertilization success rates. The results suggest that rapid dilution of gametes by turbulent mixing drastically limits the efficiency of external fertilization, with a decrease in efficiency with increasing turbulence intensities. Using parameters for the purple sea urchin *Strongylocentrotus purpuratus*, fertilization success rates are predicted in the range of only 0.01–1%. Levitan (1995) notes that if an error in the dispersion coefficients used by Denny and Shibata (1989) were corrected, then the predicted fertilization success rates would be even lower. By way of contrast, field studies for a wide range of taxa indicate that the probability of fertilization success is much higher than that predicted by the time-averaged model of Denny and Shibata (1989). The average fertilization success in the field is rarely less than 5%, and is often as high as 90%; when the nearest spawning male is closer than 1 m away, the fertilization success is typically greater than 50% (Eckman, 1996; Yund, 2000). Field observations also show high variability

in local fertilization rates, with marked variation even on scales of seconds and centimeters (Coma and Lasker, 1997). This observed variability, combined with the underpredictions of the time-averaged model, suggests that instantaneous mixing processes might play an important role in the efficiency of the broadcast spawning strategy.

Turbulent mixing of introduced chemicals, gametes, or other scalars is a result of complex instantaneous processes that occur over a range of spatial and temporal scales. For a single scalar, turbulent mixing produces a time-averaged concentration field that can be accurately described using analytical solutions to the advection–diffusion equation, where the effect of turbulence is modeled through an enhanced, effective turbulent diffusivity (Fischer et al., 1979). However, the instantaneous turbulent-mixing processes that produce the enhanced diffusivity are the subject of a rich and ongoing field of study. Mixing scenarios that involve sparse distributions of multiple scalars in chaotic turbulent flows are particularly complex, making an understanding of the broadcast spawning process at an instantaneous level difficult.

Turbulence, and turbulent mixing, is challenging to study at the instantaneous level because it is chaotic. Chaotic processes exhibit an acute sensitivity to changes in initial conditions (Pope, 2000), complicating attempts to generalize their instantaneous behavior (although their average behavior may be clear). Nonetheless, there is a vocabulary that is used to describe the effects of turbulence structure on introduced scalars. Turbulence first stirs scalars (Eckart, 1948; Garrett, 1983) into thin filament shells. The stirring process enhances local scalar gradients, and increases the interfacial area of the scalar, leading to increased mixing by molecular diffusion. The separate time scales associated with stirring and mixing dictate the resulting character of the scalar field. A blob of weakly diffusive scalars is stirred into well-defined filaments, with alternating striations of marked and unmarked fluid; the striation thickness decreases with time, but the low molecular diffusivity discourages intermingling. Alternatively, a blob of strongly diffusive scalar blurs rapidly into the surrounding unmarked fluid, and the effect of stirring may be strongly diminished. The practical extent to which a scalar is weakly or strongly diffusive depends not only on the Schmidt number of the scalar in the given fluid (i.e., the ratio of the diffusivity of fluid momentum to the diffusivity for the scalar), but also on the character of the turbulent stirring. The way in which turbulence stirs fluid, and scalars in the fluid, can be described in terms of stretching and folding of filaments (Ottino, 1989). The stretching process promotes mixing through enhancement of interfacial area, and the folding process allows the exponentially stretched material to fit into a finite space (Hinch, 1999).

An understanding of the broadcast spawning problem requires knowledge not only of how each of the two scalars (egg and sperm) evolve over space and time, but also of how they evolve relative to each other. This adds an extra layer of complexity to this problem relative to those with only a single scalar. While there are a few studies that have looked at turbulent mixing of multiple scalars (Juneja and Pope, 1996; Li and Bilger, 1996; King et al., 1997), an understanding of how multiple scalars develop in turbulent flow is relatively undeveloped.

The work presented in the present paper is motivated by the idea that turbulent stirring combined with molecular diffusion might produce spatial correlations between two passive scalars at intermediate time scales (thus enhancing fertilization efficiency), even if those scalars were not spatially correlated in the initial condition. Passive scalars do not influence the flow field, or the scalar field of other scalars, so this proposed idea can be somewhat counterintuitive. However, each scalar in a turbulent flow shares the same structured velocity field, which could produce spatial correlations in the scalar fields. The idea of turbulence *producing* correlations between passive entities in the flow is not without precedent in the literature, at least in the context of particles with slightly higher inertial characteristics than the fluid. The "focussing" of passive particles into selected regions of turbulent flows for particles with Stokes numbers greater than unity has been discussed by various researchers (Tang et al., 1992; Crowe et al., 1995; Shaw, 2003). In the present paper, we investigate this effect for hypothetical particles that are assumed to exactly follow the motion of the fluid (Stokes number equal to unity).

Stirring results from gradients in the velocity field that are associated with spatial structure. Because vortex motion is a dominant structure in turbulence, it is logical to consider stirring associated with simple

vortex flows as a way of understanding generalized turbulent stirring. In addition to accelerated scalar diffusion due to local gradient enhancement, vortex structures create spiral scalar structures that lead to a global acceleration in dissipation (Flohr and Vassilicos, 1997; Provenzale et al., 1999). Given the complexity of this problem, most studies to date have chosen to restrict the velocity field to two dimensions (Provenzale et al., 1999; Gerlinger et al., 2000). Although there are fundamental differences between two-dimensional (2D) and three-dimensional (3D) turbulence (e.g., vortex stretching, spectral distribution, energy cascade), there are still a number of fundamental similarities which justify the simplification. Within the context of understanding the role of vortex motions in turbulent mixing, these 2D flows are often further simplified to consist of just one or several idealized vortices (Aref, 1983; Babiano et al., 1994). In keeping with this growing body of literature, we employ such simplifications in the present work.

2. The role of instantaneous processes

A fundamental tenet in the study of mixing is that turbulence produces rapid dilution of introduced scalars. By extension, it has been assumed that turbulence reduces the effectiveness of broadcast spawning through rapid dilution of egg and sperm concentrations. In truth, the tenet of rapid turbulent dilution is biased by our propensity to consider only the average concentration field rather than its instantaneous structure. Consider a chemical plume with a source concentration C_0 that is introduced into a turbulent flow. As the plume is advected downstream, it is stirred (strained) into filaments by the coherent velocity structures in the flow. At the same time, molecular diffusion tends to smear out and dilute the filaments. However, for weakly diffusive scalars (characterized by high Schmidt number; this is typical of particles introduced into a flow), this molecular smearing is small relative to the turbulent stirring at short time scales. The turbulence quickly distributes the filaments over an areal extent that is large compared to the source, and the resulting spatially averaged concentration at a downstream location is small compared to C_0, suggesting rapid dilution. The time-averaged concentration at a fixed downstream location is equally small. The instantaneous scalar field, however, is more complicated. The concentration within the filaments themselves decreases quite slowly relative to the time-averaged dilution rate. For weakly diffusive scalars, turbulence is initially inefficient at producing dilution at the scale of the filaments; the turbulence merely stretches and strains the filaments into different shapes without markedly changing their concentration. It is only when these concentrated filaments are averaged with the surrounding low-concentration fluid that strong dilution is evident. In other words, the rapidity of dilution produced by turbulent mixing can appear very different to observers who view the flow with different temporal and spatial resolutions (see, e.g., Crimaldi et al., 2002a). Often, only the time-averaged concentration field (which experiences rapid dilution) is considered, biasing the perceived effect of turbulence on introduced scalars.

The contrast between the time-averaged (mean) and instantaneous concentrations in a turbulent plume is evident in the laboratory data shown in Fig. 1. The data show scalar concentrations in a thin horizontal slice through a plume of fluorescent dye in a turbulent boundary layer (see Crimaldi and Koseff, 2001; Crimaldi et al., 2002b). Fig. 1(a) is the mean concentration field (an average of 8000 images acquired at 2 Hz), where concentration strengths (normalized by the source strength) are color coded as shown in the legend. Fig. 1(b) is an enlarged snapshot (with a different color scale range) of a typical instantaneous concentration field from the boxed region delineated in Fig. 1(a). Note that the instantaneous concentration field is highly intermittent, with small filaments of high concentrations surrounded by large regions with low or zero concentration. The filaments are shaped by the turbulent velocity field. Fig. 1(c) is a comparison of lateral concentration profiles at $x = 106$ cm (shown by the dotted line). The red line is the instantaneous concentration corresponding to the instant shown in Fig. 1(b). The blue line is the mean concentration; it has a Gaussian profile. The instantaneous profile contains concentrations that can exceed the local mean concentration by several orders of magnitude. Furthermore, scalar structures having relatively high concentrations persist as the plume advects downstream, although the local mean concentration is much lower.

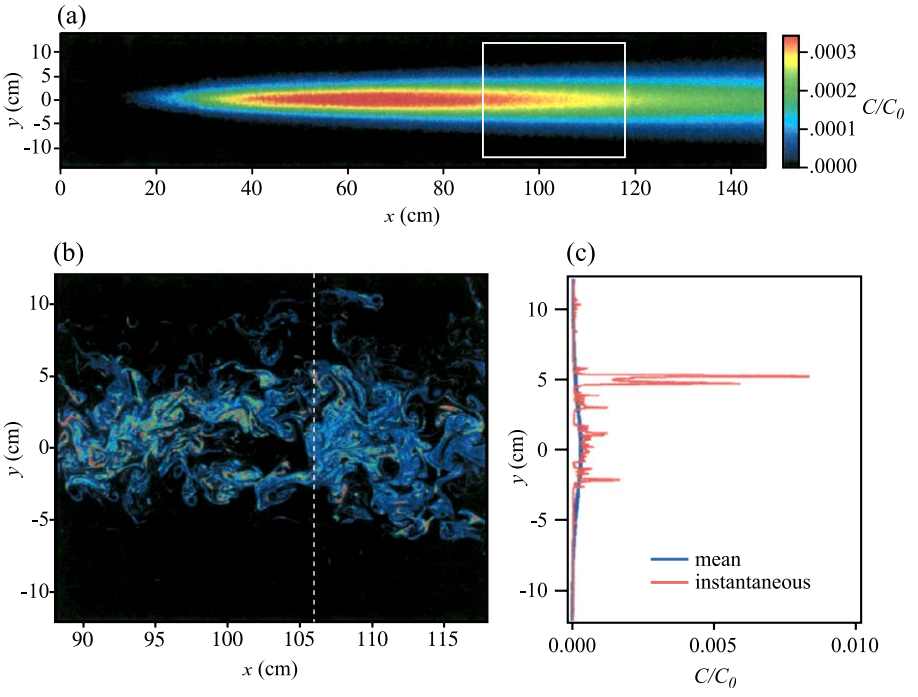

Fig. 1. Comparison of mean and instantaneous structure in a laboratory plume. Data from Crimaldi et al. (2002b).

The evolution of egg and sperm concentrations (C_e and C_s) in a turbulent plume can be modeled as the turbulent transport of two reactive chemical species (egg and sperm). Such a system is governed by a pair of coupled advection–diffusion equations (Hinze, 1959)

$$\frac{\partial C_e}{\partial t} = -\vec{u}\cdot\nabla C_e + D\nabla^2 C_e - kC_eC_s \quad (1)$$

$$\frac{\partial C_s}{\partial t} = -\vec{u}\cdot\nabla C_s + D\nabla^2 C_s - kC_eC_s \quad (2)$$

where $\vec{u}$ is the local velocity, and D is the effective turbulent scalar diffusivity. The final term in each equation is the removal of egg and sperm via fertilization. The rate of fertilization depends on the product of the co-occurring egg and sperm concentrations, multiplied by a rate constant k (Vogel et al., 1982). The local concentrations can be decomposed into the sum of the mean component (denoted by an overbar) and fluctuating component (denoted by a prime):

$$C_e(t) = \bar{C}_e + c_e'(t) \quad C_s(t) = \bar{C}_s + c_s'(t) \quad (3)$$

Substituting the concentration decompositions into the fertilization rate term kC_eC_s, and time averaging, gives

$$\overline{kC_e(t)C_s(t)} = k(\bar{C}_e\bar{C}_s + \overline{c_e'\,c_s'}) \quad (4)$$

where we have made use of the fact that $\bar{C}_e\overline{c_s'} = 0$ and $\bar{C}_s\overline{c_e'} = 0$. Thus, the average fertilization rate has two terms: the product of the local mean concentrations, plus the local correlation of the fluctuating concentration components. Previous models of broadcast spawning (e.g., Denny, 1988; Denny and Shibata, 1989) considered only the product of the means, and neglected the correlation term $\overline{c_e'c_s'}$. The correlation term is nonzero if the egg and sperm concentration fields are spatially correlated. In the following sections, we present simple conceptual and numerical models that suggest the following: (1) if egg and sperm filaments tend statistically to overlap, the resulting fertilization rates are dramatically larger than predicted by time-averaged models, and (2) coherent turbulent structures are likely to produce such statistical overlapping.

3. A conceptual model for instantaneous processes

To illustrate how instantaneous structure in scalar fields can produce a fertilization rate that differs from the rate predicted based only on time-averaged concentrations, we present a highly simplified, conceptual model of scalar coalescence. In this model, we do not consider the physical mechanisms that might produce the coalescence (these are addressed later using numerical simulations of scalar–vortex interactions). The conceptual model demonstrates the nonlinearity of the fertilization rate term kC_eC_s and provides insight to the conditions under which instantaneous processes have the largest impact on the resulting fertilization rate.

Consider two mixing scenarios each involving scalars A and B (e.g., egg and sperm). In the first, equal amounts of A and B are completely mixed throughout the entire extent of a fixed volume of water. In the second, the same masses of A and B are mixed into separate (but partially overlapping) subregions within the same fixed volume of water. In the latter scenario, the concentrations of A and B in the small subregions are high (relative to the concentrations in the first scenario), and the concentrations are zero outside the subregions. The *average* products of the concentrations $\overline{C_AC_B}$ in each of these two scenarios are generally different. Our conceptual model formalizes this disparity.

Fig. 2 illustrates the conceptual model. The large rectangle has area A_r is a representative region of the flow. Within the rectangle are subregions containing uniform concentrations of scalar A (light gray circle) and scalar B (dark gray circle); a portion of the scalar fields overlap (black region). The concentrations C_A and C_B are both unity by assumption, and the area of each circular scalar region is A_c. We now define two area-based ratios

$$r_s = \frac{A_c}{A_r} \text{ and } r_o = \frac{A_o}{A_c} \tag{5}$$

where A_o is the area of the black overlap region. Note that both r_s and r_o are constrained by definition to be between 0 and 1. Furthermore, even if $r_s \ll 1$, r_o can still have a value anywhere in the range of $0 \le r_o \le 1$. Using these assumptions and definitions, the spatially averaged product of C_A and C_B (based on the actual, nonaveraged scalar structure) is

$$\overline{C_AC_B} = \frac{1}{A_r}\iint_{A_r} C_AC_B \, dA. \tag{6}$$

Likewise, it is possible to calculate a concentration product that is based solely on the spatially averaged values of C_A and C_B, namely

$$\overline{C}_A\overline{C}_B = \frac{1}{A_r^2}\int_{A_r} C_A \, dA \int_{A_r} C_B \, dA. \tag{7}$$

Using Eqs. (4), (6) and (7), the true average concentration product $\overline{C}_A\overline{C}_B$ can be compared to the product of the average concentrations $\overline{C}_A\overline{C}_B$. A simple analysis leads to the following ratio:

$$\frac{\overline{C_AC_B}}{\overline{C}_A\overline{C}_B} = \frac{\overline{C}_A\overline{C}_B + \overline{c'_Ac'_B}}{\overline{C}_A\overline{C}_B} = \frac{r_o}{r_s}. \tag{8}$$

When the ratio is equal to unity, the true scalar product equals that calculated based on the average concentrations (because $\overline{c'_A\, c'_B} = 0$, which occurs only when $r_o = r_s$). When the ratio is greater than unity ($\overline{c'_A\, c'_B} > 0$, with $r_o > r_s$), the true product exceeds the product based on the averaged concentrations (and vice versa when the ratio is less than unity). The equation indicates that the ratio (and hence the disparity between the two averages) increases as r_o becomes large relative to r_s. Contours of the ratio defined in Eq. (8) are plotted in Fig. 3.

As an example, if scalar A and scalar B regions each comprise 2% of the representative rectangle

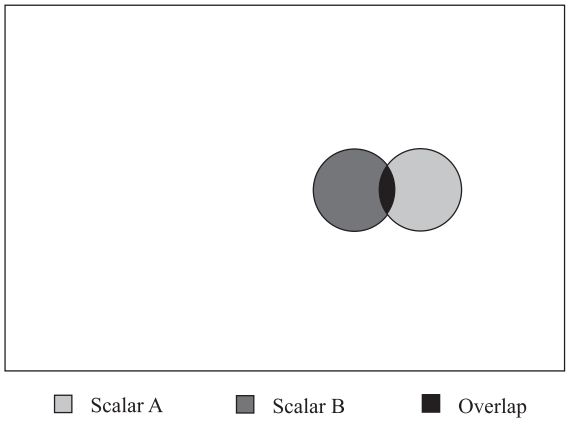

Fig. 2. Idealized filaments of two scalars (shaded regions) in a representative region of the flow (white rectangle).

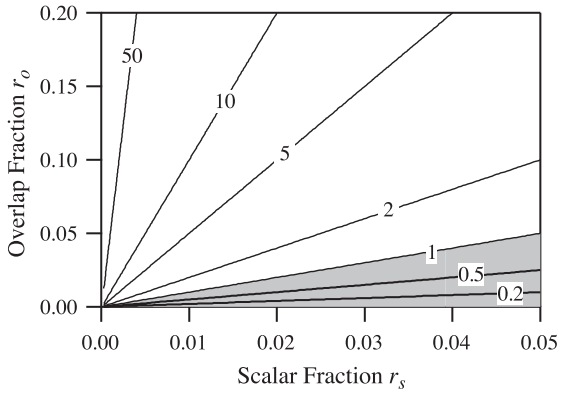

Fig. 3. Contours of the ratio $\overline{C_A C_B}/\bar{C}_A\bar{C}_B$ calculated using Eq. (8). Contours are less than unity in the shaded region.

($r_s = 0.02$), and 20% of the two regions overlap (r_o=0.2), then the true average concentration product is 10 times larger than that predicted based on averaged concentrations. The shaded region ($r_o < r_s$) corresponds to cases where the ratio is less than unity, in which case the true average concentration product is less than the product of the average concentrations.

The conceptual model does not provide any insight into the expected values of r_s and r_o, nor does it suggest how physical processes might influence these parameters. The conceptual model simply quantifies that under most circumstances ($r_o \neq r_s$), the true concentration product (and hence the true fertilization rate) cannot be predicted based on average concentrations.

4. Analytical modeling of diffusive scalar overlap

Molecular diffusion is necessary in order for any overlap (i.e., A_o>0 in Fig. 2) to exist between two scalars that have nonoverlapping initial conditions ($A_o = 0$). From a process-based approach, therefore, it is logical to examine the effect of pure diffusion (i.e., no stirring) on the temporal evolution of scalar coalescence. This approach also corresponds to a purely time-averaged view of turbulent mixing, where the effect of turbulence is modeled by an effective diffusivity. We consider two scalar point sources, initially located a distance L apart. Each source has a scalar mass M, with one source being scalar A, and the other scalar B; both have the same diffusivity D (either molecular or turbulent). As time progresses, the mass at each point diffuses radially outward, and overlap between the two scalars develops (i.e., $C_A C_B$ becomes nonzero). The analytical solution for 2D diffusion of a scalar mass M initially located at $x_1 = \xi_1$, $x_2 = \xi_2$ is (Fischer et al., 1979)

$$C(t) = \frac{M}{4\pi D t}\exp\left[-\frac{(x_1-\xi_1)^2 + (x_2-\xi_2)^2}{4Dt}\right]. \quad (9)$$

We define the total concentration overlap as

$$\Theta(t) = \int\int C_A C_B \, \mathrm{d}A \quad (10)$$

Note that $\Theta(t)$ is a measure of the potential fertilization rate at a given time. Eqs. (9) and (10) can be used to form the following analytical expression for the temporal evolution of the product of two diffusive concentration fields:

$$\Theta_D(t) = \frac{M^2}{8\pi D t}\exp\left[-\frac{L^2}{8Dt}\right]. \quad (11)$$

The maximum value of Eq. (11), and the time in which the maximum occurs, can be used to form the following nondimensional Θ and t variables:

$$\Theta^* = \frac{\pi e L^2}{M^2}\Theta \text{ and } t^* = \frac{8D}{L^2}t. \quad (12)$$

These variables can then be used rewrite Eq. (11) in a nondimensional form as

$$\Theta_D^* = \frac{e}{t^*}\exp\left[-\frac{1}{t^*}\right]. \quad (13)$$

A plot of Θ_D^* vs. t^* is shown in Fig. 4. Initially, the two sources are distinct, and there is no overlap. As the scalars diffuse, they begin to overlap, and Θ_D^* becomes nonzero. As the diffusion continues, there is a larger and larger region with overlapping scalars, but the diffusion is also causing all of the large concentrations to decrease in magnitude. Thus, Θ_D^* reaches a peak value, and then decays monotonically. In the limit as $t^* \rightarrow \infty$, the spatial extent of the two scalar fields becomes indistinguishable, but the concentrations have also everywhere tended to zero, resulting in $\Theta_D^* = 0$. From a broadcast spawning standpoint, this result suggests that diffusion can have competing

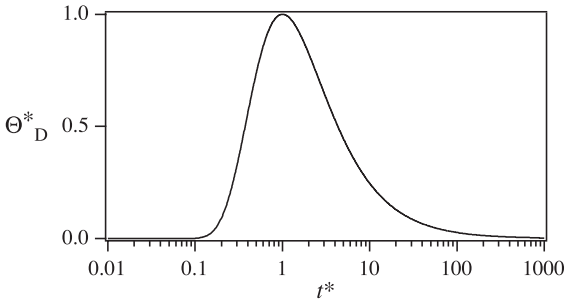

Fig. 4. Evolution of nondimensional scalar overlap for pure diffusion of two scalar sources.

effects on successful fertilization. Diffusion is required to bring the scalars together, and promotes fertilization for $t^*<1$. However, diffusion dilutes the large, central concentrations, and, for $t^*>1$, hinders fertilization.

To some extent, many of these same arguments could be extended to an effective turbulent diffusivity for turbulent flows. However, turbulence imposes a new, and critical, phenomenon into the process: instantaneous stirring action. We now use a simple numerical model to investigate the effect of stirring via scalar–vortex interactions.

5. Numerical modeling of scalar–vortex interactions

We developed a simple numerical model to investigate interactions between discrete vortices and the coalescence of two scalars such as egg and sperm. The models use particle-tracking techniques to follow the paths of individual egg and sperm in idealized flows consisting of one or more free vortex. Particle-tracking methods have been widely used in previous studies (Awaji, 1982; Dimou and Adams, 1993; Scott, 1997), and have been shown to offer computational efficiency and simplicity unavailable in finite-element or finite-difference alternatives (Tompson and Gelhar, 1990). In the particle-tracking method, the two-dimensional position of a particle $\vec{x}_n$ is determined from its previous position $\vec{x}_{n-1}$ using the updating relationship (Kinzelbach, 1988; Hathhorn, 1997).

$$\vec{x}_n = \vec{x}_{n-1} + \vec{u}(\vec{x}_{n-1})\Delta t + \vec{Z}\sqrt{2D\Delta t} \tag{14}$$

where $\vec{u}(\vec{x}_{n-1})$ is the local velocity vector at position $\vec{x}_{n-1}$, D is the diffusivity, and $\vec{Z}$ is a two-dimensional vector of random numbers with mean magnitude zero and variance one. Two advantages of the random walk particle-tracking method are that it does not exhibit any numerical dispersion in the classical sense (Kinzelbach, 1988) and that computational effort is proportional to the number of particles and concentrated into areas with the highest concentrations (Dimou and Adams, 1993). For investigations of broadcast spawning, the technique has the additional advantage in that it allows the positions of discrete particles to be tracked individually.

Real turbulence consists of three-dimensional vortical motions that strain introduced contaminants into filaments that ultimately are diluted by molecular diffusion. In our model, we use highly simplified, idealized vortex flows in two dimensions to investigate the role of vortical motion on the coalescence of egg and sperm at intermediate time scales. Our model uses one or more ideal vortices as an idealized flow that mimics the behavior in the outer regions of real vortices found in turbulence. The ideal vortex flow field is given by

$$u_\theta = \frac{a}{r} \tag{15}$$

where a is a constant that determine the rotational strength of the vortex (i.e., the total circulation). Fig. 5 shows a vector plot of the two-dimensional velocity distribution for a single ideal vortex located at the origin. Note that an ideal vortex has no intrinsic length scale—the vortex is completely defined by the rotational strength parameter a. The ideal vortex also does not have an intrinsic time scale, although one can be calculated for a given radius. The rotational frequency at $r=R$ is given by

$$\omega_R = \frac{a}{2\pi R^2} \tag{16}$$

which serves as an (inverse) time scale for the vortex in the vicinity of $r=R$. This time scale is used in a subsequent dimensional analysis. The first case modeled contains a single vortex, and the second case contains three interacting vortices. In each of the two cases, separate parcels of egg and sperm are placed in the flow field and allowed to advect and evolve over

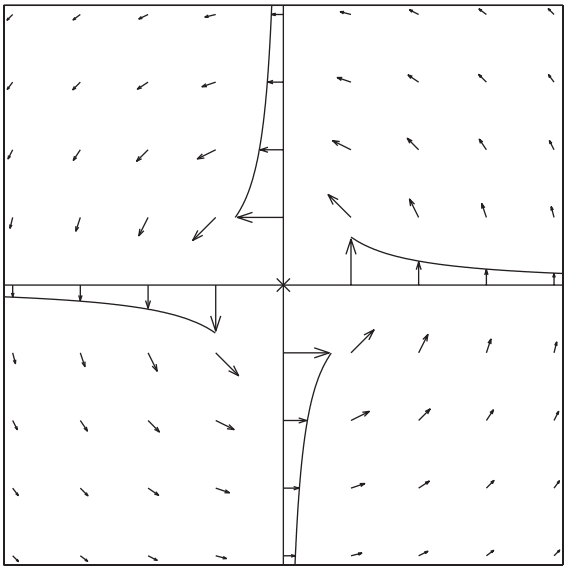

Fig. 5. Velocity vectors for an ideal vortex (Eq. (15)).

time. For simplicity, we do not include a fertilization kinetics model—that is, the particles are conservative. Our objective is simply to identify turbulent mechanisms that influence the coalescence of egg and sperm.

5.1. Single-vortex case

The first case utilizes a flow consisting of a single, free vortex centered on the origin. Fig. 6 shows the geometry of the initial condition. Note that the view in Fig. 6 is the same as Fig. 5. Points A and B indicate the initial locations of the two scalar masses, each located a distance $L/2$ from the vortex center, which is indicated by the $\times$ symbol. The two scalars always start out on opposite sides of the vortex center. For the numerical simulations, a total of 80,000 particles are used, with $N_p = 40{,}000$ particles used for each of the two scalars A and B. Each particle is assumed to have a scalar mass of M/N_p, so that each scalar has a total mass of M. Particle locations for $t>0$ are determined by numerically integrating Eqs. (14) and (15) over time. Concentration maps are calculated from the resulting particle locations by imposing a 100×100 grid over the domain and grouping particles into discrete two-dimensional bins. Separate concentration maps are made for each scalar, and these concentration maps are multiplied and integrated according to Eq. (10) to calculate Θ at each time step.

The simple geometry and flow field of our simulation lends itself to a dimensional analysis that predicts the relevant nondimensional parameters which control the magnitude of Θ. The assumed functionality

$$\Theta = f(L, D, M, \omega, t) \tag{17}$$

leads directly to a nondimensional functional relationship

$$\frac{\pi e L^2}{M^2}\Theta = f\left(\frac{8Dt}{L^2}, \frac{\omega L^2}{8D}\right). \tag{18}$$

Using the notation introduced in Eq. (12), this functionality becomes

$$\Theta^* = f(t^*, P) \tag{19}$$

where $P = \omega L^2/8D$. Thus, the nondimensional scalar overlap in our simple formulation will depend only on t^* and P. The parameter t^* is a ratio of the elapsed simulation time to the time scale required for either scalar to diffuse a distance $L/2$. The

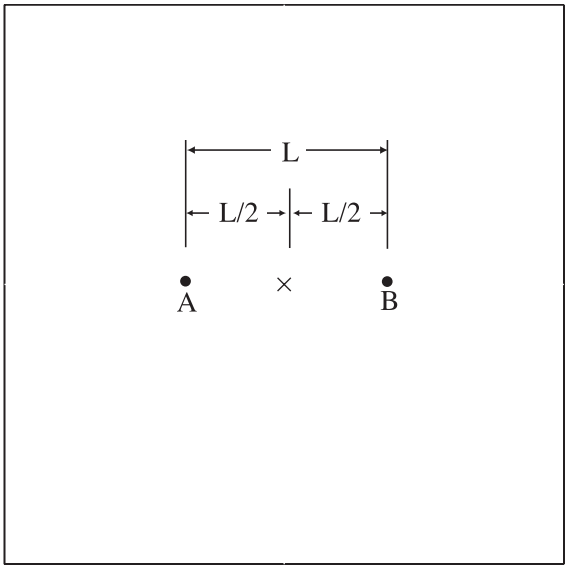

Fig. 6. Single-vortex model initial condition. Vortex center is indicated by the $\times$ symbol. Points "A" and "B" indicate the initial locations of scalars A and B.

parameter P is a ratio of this same diffusive time to the time required for one complete vortex revolution at $r = L/2$.

To groundtruth the diffusion implementation in the model, we first ran a simulation with no vortex velocities (i.e., $a = 0$ in Eq. (15)). This corresponds to the pure diffusion case described by the analytical model in Section 4 and to the limiting case $P = 0$ in our dimensional analysis. Fig. 7 shows a time series of the spatial evolution of particles of scalars A (red) and B (blue). Only a representative portion of the total number of particles used in the simulation are plotted. In the first frame ($t^* = 0.02$), the particles have diffused only a short distance from their initial locations. In subsequent frames, the particles further diffuse and intermingle. Values of the nondimensional scalar overlap Θ^* for $P = 0$ calculated from the model are shown in Fig. 9 (circle symbols). The model results are in agreement with the analytical prediction for the pure diffusive case (Eq. (13)), which is also shown in the figure (solid line).

We now add the effect of the vortex–scalar interaction by setting $P > 0$. Fig. 8 shows the evolution of particle positions for the case $P = 10$. This means that the vortex will have rotated 10 times (at $r = R$) by time $t^* = 1$, at which point a typical particle will have diffused a distance $L/2$. The "interesting" physics now occur at much shorter values of t^*, relative to the $P = 0$ case. This is due to the inclusion of the new (faster) time scale ω. Thus, the time series in Fig. 8 is shown at time intervals that are 10 times shorter than those used in Fig. 7. The images also show the formation of scalar filaments by the radial shear in the circumferential velocity. These filaments are brought rapidly (relative to the diffusion time scale) into close proximity, at which point diffusion is able to bridge the short gap to produce the scalar overlap. Resulting values of the nondimensional scalar overlap Θ^* for $P = 10$ as well as several other P values are shown in Fig. 9. As P increases, the peak scalar overlap gets larger, and it comes sooner in time. Both of these trends indicate an increase in fertilization success as P increases.

The addition of the structured vortex field ($P > 0$) results in a higher scalar overlap (and hence fertilization rate) than would result from pure diffusion (whether the diffusion was molecular or turbulent). Thus, the scalar overlap resulting from the vortex flow is larger than that predicted by a time-averaged model that used an equivalent turbulent diffusivity to represent the turbulence, regardless of the magnitude of the diffusivity.

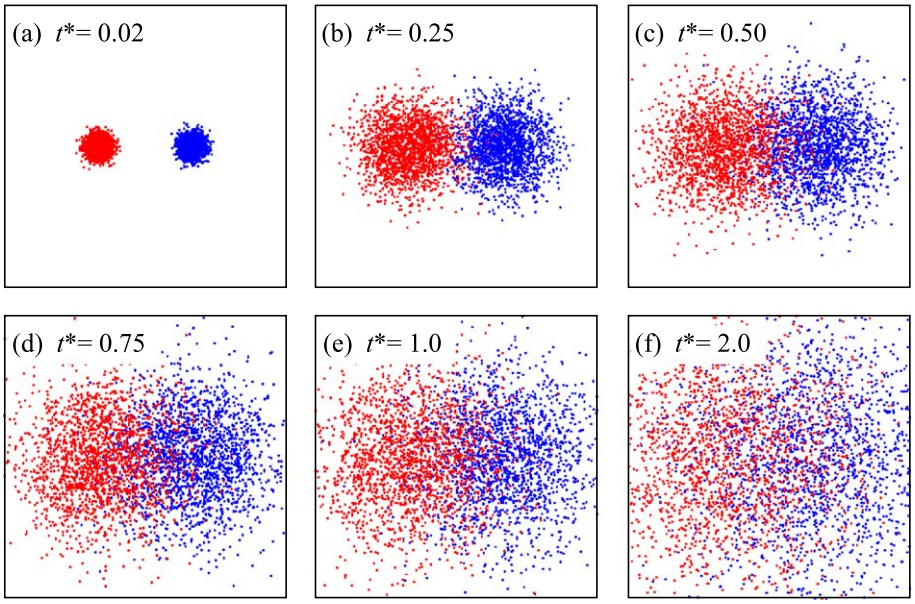

Fig. 7. Particle evolution in the single-vortex model for $P = 0$ (pure diffusion).

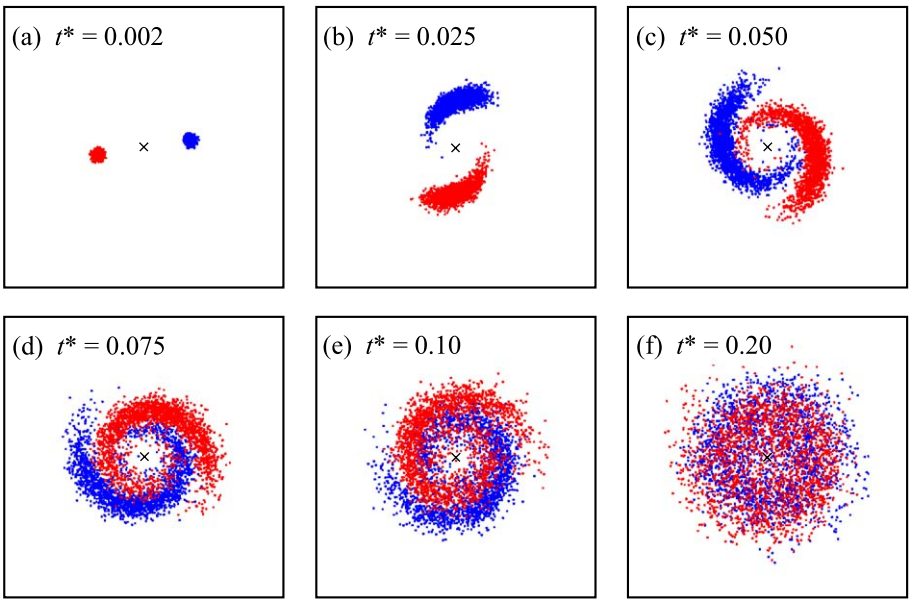

Fig. 8. Particle evolution in the single vortex model for $P = 10$ (diffusion and stirring). Time frames shown are 10 times sooner than those shown in Fig. 7.

Θ^* continues to grow larger as P is increased. This result does not rely on the symmetric initial condition used in our model; in fact, slightly higher Θ^* values are achieved when a small amount of eccentricity is added to the initial condition. As $t^* \rightarrow \infty$, the structure of the initial scalar condition is lost, and the problem degenerates (for all values of P) back to the pure diffusion case. The large-time behavior of the scalar overlap for the pure diffusion case can be found by taking the time limit of Eq. (13), which gives

$$\Theta^*_\infty = \frac{e}{t^*}. \tag{20}$$

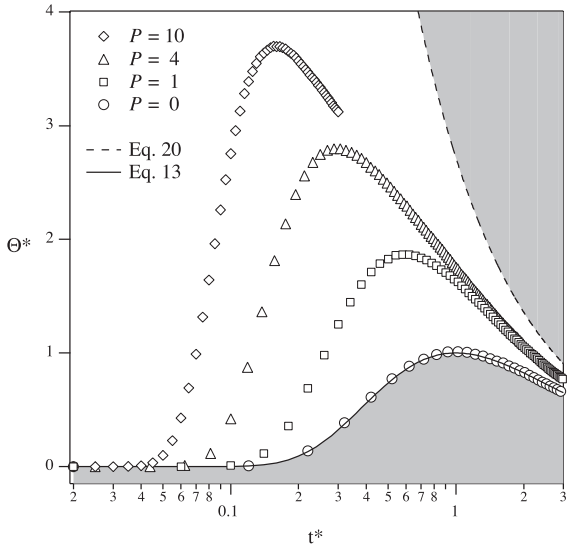

Fig. 9. Nondimensional scalar overlap Θ^* vs. t^* for various values of P.

Eq. (20) is shown along with the model results in Fig. 9, and is seen to represent the upper bound of the large-time overlap behavior. The shaded areas in the figure delineate the envelope of possible results for our single-vortex model.

5.2. Three-vortex case

We extended the configuration of the numerical model to include the interacting effect of more than one vortex. The results in this section are qualitative in nature, and serve to illustrate the increased complexity that occurs in chaotic flows. For simplicity, three equal strength, same sign, ideal vortices are used, and molecular diffusion is neglected ($D = 0$, so that $P = \infty$). Although this choice removes all time scales from the problem, it allows the effect of stirring

to be examined in a pure form. The three vortices interact with one another through mutual induction (Panton, 1996), and the resulting flow field exhibits chaotic behavior (Aref, 1983). The initial condition and subsequent particle locations are shown as a sequential series of frames in Fig. 10. The initial egg (red) and sperm (blue) parcel locations, as well as the initial vortex locations (× symbols) are shown in frame (a). In subsequent frames, the egg and sperm particles, as well as the vortices themselves, move in response to the combined effect of the three vortices. Once again, the strain rates associated with the vortices stir the egg and sperm into long filaments (b, c). Although the details are more complex, processes similar to those seen in the first single-vortex model are evident. The coherent velocity structures cause filaments of egg and sperm to coalesce with remarkable efficiency (d, e, f). Because $D=0$ in the simulation, the filaments never technically overlap, but the addition of even a small amount of diffusivity would allow efficient overlap to rapidly occur. The spatial coherence of the velocity field generates spatial correlations between the egg and sperm concentration fields, although the egg and sperm particles have no knowledge of one another. Because of the nonlinear nature of the fertilization rate kC_eC_s, these overlapping regions of high egg and sperm concentrations correspond to regions of extremely high fertilization rates. However, due to the chaotic nature of the setup, small changes in the initial condition produce very different results, and not all simulations produce coalescence that is as dramatic as that shown here. This work needs to be extended further before the net quantitative effect of the turbulence is known.

6. Discussion

6.1. Physical and biological context of the models

The analytical and numerical models used in this study are intentionally simple representations of a complex process involving coupled physical–biological phenomena. The goal of the study is to use simple models to reveal basic physical processes that control the efficiency of broadcast spawning. The results of the investigation are qualitative rather than quantitative, and suggest directions for future research rather than providing definitive explanations. It is therefore useful to first discuss the models and their simplifi-

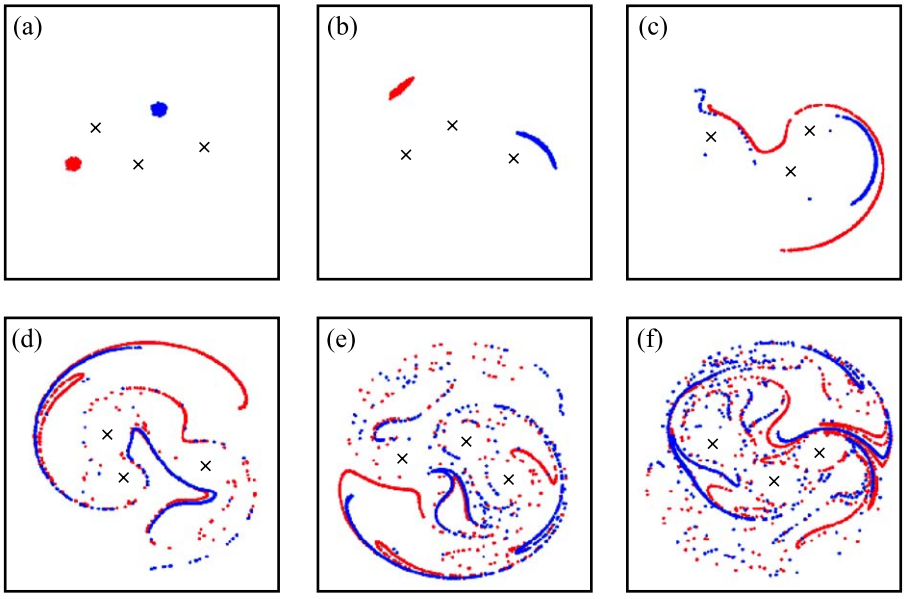

Fig. 10. Evolution of parcels of egg (red) and sperm (blue) placed in the vicinity of three ideal vortices, all with counterclockwise rotation. The center of each vortex is shown by a × symbol. Individual frames are spaced equally in time.

cations in the context of their real physical and biological counterparts.

Turbulence is notoriously complex, but consists at the most basic level of a superposition of simple vortical motions. The vortex formulations used in this study are idealized, but share many of the characteristics of real vortices, especially in their capacity to stir scalars into filaments. Although the simple formulations do not capture the three-dimensional structure and temporal evolution of vortical motions in real turbulence, they do capture the essence of the motion at local scales. The coalescence processes observed in the simple models are certainly present in real turbulence, albeit to a possibly greater or lesser extent. Vortex stretching, which is intrinsic to three-dimensional turbulence, is an example of a process that is potentially important, but not modeled in our two-dimensional pseudoturbulence. Future models should also investigate the effect of more than three vortices, as well as vortices with unequal strengths and rotational sense.

The particle-tracking approach used in the numerical models is particularly well suited for this study. The model computes the paths of individual particles based solely on advection by the flow and molecular diffusion. These two mechanisms control the motion of egg and sperm at all but the smallest scales, where sperm motility may play a role. Sperm motility and taxis would produce an increase in the effective diffusivity of the sperm, but with a selective direction (towards nearby eggs). This effect seems likely to enhance the coalescence processes observed in our study. It is important to note that our study does not incorporate any reaction kinetics model. That is, there is no actual fertilization, and there is no postfertilization removal of viable egg or sperm from the system. This simplification is a shortcoming only in the sense that we do not end up quantifying the resulting fertilization rates. We do succeed in demonstrating the physical processes that bring the gametes together in concentrated filaments, and provide analytical evidence that this would result in greatly enhanced fertilization rates relative to a well-mixed, time-averaged system. A move towards incorporating reaction kinetics requires an understanding of the relationship between the time scales of the biological and physical aspects of coupled process. A qualitative discussion of the relevant time scales in the physical processes, and the relationship to the biological processes, is given in the following section.

6.2. From stirring to mixing: the relevance of time scales

The simple models developed in this study reveal that the physical stirring and mixing process progresses through several temporal regimes, each with qualitatively distinct implications for the egg and sperm concentration fields. The time scales of these regimes, and the relationship between these time scales and those in the biological process, are critical to the overall effectiveness of broadcast spawning. The importance of time scales is particularly well illustrated by Eq. (18), which formulates our simple model in terms of the time scales associated with diffusion and straining.

The first temporal regime occurs at time scales that are short relative to the time scale required for the turbulence to produce significant local dilution of egg and sperm ($t^* \ll 1$). In this regime, parcels of recently extruded egg and sperm are stretched and strained by local velocity gradients into the beginnings of filaments. Concentrations within the parcels remain relatively unchanged during this initial stirring. Frames (a) and (b) in Figs. 8 and 10 are representative of this initial regime. The second regime occurs at what we will call intermediate time scales ($t^* < 1$). In this regime, the egg and sperm parcels are stirred into long filaments, spreading them out over significant regions of space. Molecular diffusion has the opportunity to produce some dilution in the filaments due to the greatly enhanced interfacial area between the filaments and the surrounding fluid. However, the concentrations remain quite high in the filaments (and it is only in a spatial or temporal average of the flow that significant dilutions are seen). The unique feature of this regime is the coalescence of egg and sperm filaments within coherent structures of the flow. Frames (c), (d), and (e) are representative of these intermediate time scales. The final regime occurs at time scales that are comparable or long relative to the time required for true local dilution ($t^* > 1$). At this point, enough time has passed so that the highly stirred filaments begin to lose their structure due to smearing by molecular diffusion. The end-state of the turbulent mixing process is a uniform

dilution of egg and sperm over the entire local region of interest. This end state corresponds exactly to the time-averaged concentrations used in previous models of broadcast spawning. This final regime is starting to form in frame (f), but actually extends well beyond the limited time span of our models.

The intermediate time scales, as defined above, are critical to efficient fertilization in the broadcast spawning process. At short time scales, there is little or no coalescence of the egg and sperm. At long time scales, the situation degenerates into a well-mixed, highly diluted set of egg and sperm concentrations that, although overlapped, would produce low fertilization rates due to the nonlinearity in the fertilization rate term. The intermediate time scales are the most productive, because the concentrations are still relatively large, and there is significant coalescence between the filaments.

What time scale ratios might be typical of real flow situations where broadcast spawning is occurring? It is difficult to generalize, but it is easy to choose a range of realistic parameters that produce values of P that are significantly larger than unity. In this case, the results shown in Fig. 9 suggest that the scalar overlap (and hence the fertilization rate) would be much larger than the overlap predicted by a time-averaged diffusion process (regardless of the value of the turbulent diffusivity used). It is interesting to note that broadcast spawning species may have developed strategies to prolong the length of the intermediate time scales to provide more time for fertilization before severe dilution occurs. A strategy for extending the intermediate time scales would have to hinder local dilution without disrupting the ability for filaments to coalesce. Thomas (1994) measured the physical properties of gametes for three sea urchin species and found all to be highly viscous, with the highest viscosity belonging to the species that lived in the most turbulent flow regime. Thomas (1994) hypothesizes that the high viscosity might allow strands of gametes to clump on solid surfaces, enhancing fertilization. In the context of the present study, the viscous nature of the gamete strands could slow local dilution without preventing filament coalescence, therefore providing an enhancement mechanism within the flow itself.

The results of the single-vortex model (Fig. 9) suggest that as the amount of stirring relative to diffusion (as parameterized by P) increases, so does the maximum scalar overlap (which is considered a measure of the potential fertilization rate). The model therefore predicts that more stirring is always a benefit to fertilization. However, the time scale at which the maximum occurs also comes much more quickly as stirring is increased. This could impose constraints from a biological perspective, therefore, because the time scales of the biological fertilization process must also be considered. In addition, the increase in stirring can have other detrimental effects, such as gamete mortality associated with shear (Mead and Denny, 1995).

The unifying theme of this study, and the most important result, is that the perception of complex processes like broadcast spawning (and therefore the realism of models) depends largely on the spatial and temporal scales from which the problem is viewed. This study suggests that the most important time scales for broadcast spawning are those which are long relative to the time required to stir egg and sperm parcels into filaments, but short compared to those required to produce true local dilution of the concentrations. Any model that is ultimately successful at predicting actual fertilization success rates will have to identify, and be able to resolve, these time scales.

Acknowledgements

The authors would like to thank Jeffrey B. Weiss for suggestions regarding the mathematical formulation of the ideal vortex system. We also thank Andrew Edwards and an anonymous reviewer for their efforts in improving the manuscript.

References

Aref, H., 1983. Integrable, chaotic, and turbulent vortex motion in two-dimensional flows. Annu. Rev. Fluid Mech. 15, 345–389.

Atkinson, O., Yund, P., 1996. The effect of variation in population density on male fertilization success in a colonial ascidian. J. Exp. Mar. Biol. Ecol. 195, 111–123.

Awaji, T., 1982. Water mixing in a tidal current and the effect of turbulence on tidal exchange through a strait. J. Phys. Oceanogr. 12, 501–514.

Babiano, A., Boffetta, G., Provenzale, A., Vulpiani, A., 1994. Chaotic advection in point vortex models and two-dimensional turbulence. Phys. Fluids 6, 2465–2474.

Byrd Jr., E., Collins, F. 1975. Absence of fast block to polyspermy in eggs of the sea urchin *Strongylocentrotus purpuratus*. Nature 257, 675–677.

Claereboudt, M., 1999. Fertilization success in spatially distributed populations of benthic free-spawners: a simulation model. Ecol. Model. 121, 221–233.

Coma, R., Lasker, H., 1997. Effects of spatial distribution and reproductive biology on in situ fertilization rates of a broadcast-spawning invertebrate. Biol. Bull. 193, 20–29.

Crimaldi, J., Koseff, J., 2001. High-resolution measurements of the spatial and temporal structure of a turbulent plume. Exp. Fluids 31, 90–102.

Crimaldi, J., Koehl, M., Koseff, J., 2002a. Effects of the resolution and kinematics of olfactory appendages on the interception of chemical signals in a turbulent odor plume. Environ. Fluid Mech. 2, 35–63.

Crimaldi, J.P., Wiley, M.B., Koseff, J.R., 2002b. The relationship between mean and instantaneous structure in turbulent passive scalar plumes. J. Turbul. 3, 1–24 (http://stacks.iop.org/JoT/3/014).

Crowe, C., Troutt, T., Chung, J., Davis, R., Moore, E., 1995. A turbulent flow without particle mixing. Aerosol Sci. Tech. 22, 135–138.

Csanady, G., 1973. Turbulent Diffusion in the Environment. Reidel, Boston.

Denny, M., 1988. Biology and the Mechanics of the Wave-Swept Environment. Princeton Univ. Press, Princeton, NJ.

Denny, M.W., Shibata, M.F., 1989. Consequences of surf-zone turbulence for settlement and external fertilization. Am. Natur. 134, 859–889.

Denny, M., Dairiki, J., Distefano, S., 1992. Biological consequences of topography on wave-swept rocky shores: I. Enhancement of external fertilization. Biol. Bull. 183, 220–232.

Dimou, K., Adams, E., 1993. A random-walk, particle tracking model for well-mixed estuaries and coastal waters. Estuar. Coast. Shelf Sci. 37, 99–110.

Eckart, C., 1948. An analysis of the stirring and mixing processes in incompressible fluids. J. Mar. Res. 7, 265–275.

Eckman, J.E., 1996. Closing the larval loop: linking larval ecology to the population dynamics of marine benthic invertebrates. J. Exp. Mar. Biol. Ecol. 200, 207–237.

Fischer, H., List, E., Koh, R., Imberger, J., Brooks, N., 1979. Mixing in Inland and Coastal Waters. Academic Press, San Diego, CA.

Flohr, P., Vassilicos, J., 1997. Accelerated scalar dissipation in a vortex. J. Fluid Mech. 348, 295–317.

Garrett, C., 1983. On the initial streakiness of a dispersing tracer in two- and three-dimensional turbulence. Dyn. Atmos. Ocean. 7, 265–277.

Gerlinger, W., Schneider, K., Falk, L., Bockhorn, H., 2000. Numerical simulation of the mixing of passive and reactive scalars in two-dimensional flows dominated by coherent vortices. Chem. Eng. Sci. 55, 4255–4296.

Giese, A., Pearse, J. (Eds.), 1974. Reproduction of Marine Invertebrates, Vol. 1. *Acoelomate* and *Pseudocoelomate Metazoans*. Academic Press, New York, pp. 1–49. Ch. Introduction.

Gray, J., 1955. The movement of sea-urchin spermatozoa. J. Exp. Biol. 32, 775–801.

Hathhorn, W., 1997. Simplified approach to particle tracking methods for contaminant transport. J. Hydraul. Eng. 123, 1157–1160.

Hinch, E., 1999. Mixing: turbulence and chaos—an introduction. In: Chaté, H., Villermaux, E., Chomaz, J. (Eds.), Mixing: Chaos and Turbulence. Kluwer Academic Publishing/Plenum, New York, pp. 37–56.

Hinze, J., 1959. Turbulence. McGraw-Hill, New York.

Juneja, A., Pope, S., 1996. A dns study of turbulent mixing of two passive scalars. Phys. Fluids 8, 2161–2184.

King, G., Lucht, R., Dutton, J., 1997. Quantitative dual-tracer planar laser-induced fluorescence measurements of molecular mixing. Opti. Lett. 22, NN633N–NN635N.

Kinzelbach, W., 1988. The random walk method in pollutant transport simulation. In: Custodio, E. (Ed.), Groundwater Flow and Quality Modeling. D. Reidel Publication, Rotterdam, pp. 227–245.

Levitan, D., 1993. The importance of sperm limitation to the evolution of egg size in marine invertebrates. Am. Natur. 141, 517–536.

Levitan, D., 1995. The ecology of fertilization in free-spawning invertebrates. In: McEdward, L. (Ed.), Ecology of Marine Invertebrate Larvae. CRC Press, Boca Raton, FL, pp. 123–156.

Levitan, D., Young, C., 1995. Reproductive success in large populations: empirical measures and theoretical predictions of fertilization in the sea biscuit *Clypeaster rosaceus*. J. Exp. Mar. Biol. Ecol. 190, 221–241.

Levitan, D., Sewell, M., Chia, F., 1991. Kinetics of fertilization in the sea urchin *Strongylocentrotus franciscanus*: interaction of gamete dilution, age, and contact time. Biol. Bull. 181, 371–378.

Levitan, D., Sewell, M., Chia, F., 1992. How distribution and abundance influence fertilization success in the sea urchin *Strongylocentrotus franciscanus*. Ecology 73, 248–254.

Li, J., Bilger, R., 1996. The diffusion of conserved and reactive scalars behind line sources in homogeneous turbulence. J. Fluid Mech. 318, 339–372.

Mead, K., Denny, M., 1995. The effects of hydrodynamic shear stress on fertilization and early development of the purple sea urchin *Strongylocentrotus purpuratus*. Biol. Bull. 188, 46–56.

Miller, R., 1985. Demonstration of sperm chemotaxis in echinodermata: asteroidea, holothuroidea, ophiuroidea. J. Exp. Zool. 234, 383–414.

Ottino, J., 1989. The Kinematics of Mixing: Stretching, Chaos, and Transport. Cambridge Univ. Press, Cambridge.

Panton, R., 1996. Incompressible Flow. Wiley, New York.

Pennington, J., 1985. The ecology of fertilization of echinoid eggs: the consequences of sperm dilution, adult aggregation, and synchronous spawning. Biol. Bull. 169, 417–430.

Pope, S.B., 2000. Turbulent Flows. Cambridge Univ. Press, Cambridge.

Provenzale, A., Babiano, A., Zanella, A., 1999. Mixing: turbulence and chaos—an introduction. In: Chaté, H., Villermaux, E., Chomaz, J. (Eds.), Mixing: Chaos and Turbulence, pp. 207–228 Kluwer Academic Publishing/Plenum, New York.

Scott, C., 1997. Particle tracking simulation of pollutant discharges. J. Environ. Eng. 123, 919–927.

Shaw, R.A., 2003. Particle-turbulence interactions in atmospheric clouds. Annu. Rev. Fluid Mech. 35, 183–227.

Styan, C., 1998. Polyspermy, egg size, and the fertilization kinetics of free-spawning marine invertebrates. Am. Natur. 152, 290–297.

Tang, L., Wen, F., Yang, Y., Crowe, C., Chung, J., Troutt, T., 1992. Self-organizing particle dispersion mechanism in a plane wake. Physics of Fluids. A, Fluid Dyn. 4 (10), 2244–2251.

Thomas, F., 1994. Physical properties of gametes in three sea urchin species. J. Exp. Biol. 194, 263–284.

Tompson, A., Gelhar, L., 1990. Numerical simulation of solute transport in three-dimensional, randomly heterogeneous porous media. Water Resourc. Res. 26, 2541–2562.

Vogel, H., Czihak, G., Chang, P., Wolf, W., 1982. Fertilization kinetics of sea urchin eggs. Math. Biosci. 58, 189–216.

Yund, P., 2000. How severe is sperm limitation in natural populations of marine free-spawners? Trends Ecol. Evol. 15, 10–13.